RELIABILITY ASSESSMENT OF WAFER LEVEL PACKAGE USING ARTIFICIAL NEURAL NETWORK REGRESSION MODEL

P. H. Chou K.N. Chiang*

Advanced Microsystem Packaging and Nano-Mechanics Research Lab, Taiwan
Dept. of Power Mechanical Engineering, National Tsing Hua University,
Hsinchu, Taiwan, R.O.C.

Steven Y. Liang

Georgia Institute of Technology,
George W Woodruff School of Mechanical Engineering,
Atlanta, USA

ABSTRACT

For electronic packaging structure, there are many design parameters that will affect its reliability performance, using experimental way to obtain the reliability result will take a considerable amount of time. Therefore, how to shorten the design time becomes a critical issue for new electronic packaging structure development. This research will combine artificial intelligence (AI) and simulation technology to assess the long-term reliability of wafer level packaging (WLP). A simulation technology using finite element method (FEM) with appropriate mechanics theories has been validated by multiple experiments will replace the experiment to create reliability results for different WLP structures. After a big WLP structure-reliability database created, this study will apply artificial neural network (ANN) theory to analyze this database and obtains a regression model for structure-reliability relationship of WLP. Once the regression model is established and validated, the WLP geometry, such as pad size, die and buffer layer thickness, and solder volume, etc. can be simply entered, and then the WLP reliability results can be immediately obtained through the ANN regression model.

Keywords: FEM simulation, WSP, Machine learning, Artificial neural network, Regression model

1. INTRODUCTION

In recent years, artificial intelligence theory has been widely used in various research domains. Machine learning [1] is to use AI theory combined with big data to guide computers for training and learning and finally concluded a model to help researchers make decisions. Machine learning can be applied for regression or classification model using either unsupervised or supervised learning.

McCulloch and Pitts [2] proposed an ANN method for multilayer neural networks. This method is based on the concept of the brain's self-thinking learning, mimicking the human nervous system to process information. As shown in Fig. 1, the data is entered at the input layer and then calculated in the hidden layer. Once the calculation is complete, the results are displayed in the output layer. Artificial neural networks have the ability to handle complex data, deep learning, and can efficiently handle complex nonlinear and multivariate relationships. Compared with other machine learning methods, artificial neural networks can adjust weightings, deviations and hidden values, and change some parameters, such as the number of neurons in the hidden layer and the number of hidden layers to obtain a good regression model. Of course, if the parameters are not properly adjusted, problems such as overfitting and inaccuracy will occur.

This study is mainly to apply artificial neural networks to learn and establish a regression model for the relationship of input data and output result. The experimentally varified finite element simulation methodology combined with the Coffin-Manson empirical equation for reliability prediction are used to estimate the fatigue life of the solder joint of WLP.

* Corresponding author (knchiang@pme.nthu.edu.tw *)

DOI : 10.1017/jmech.2019.20
Copyright © 2019 The Society of Theoretical and Applied Mechanics

https://doi.org/10.1017/jmech.2019.20 Published online by Cambridge University Press

Table 1 Dimension of WLP TV1 & TV2

Material	TV1(mm)	TV2(mm)
Si Chip	5.3x5.3x0.33	4x4x0.33
Cu RDL	0.26x0.008	0.26x0.008
UBM	--	0.24x0.0086
Cu Pad	0.22x0.025	0.22x0.025
SBL1	5.3x5.3x0.0075	4x4x0.0075
SBL2	0.01	0.004
PCB	10.6x10.6x1	8x8x1
Low-k	5.3x0.005	4x0.005

Table 2 Dimension of WLP TV3 & TV4

Material	TV3(mm)	TV4 (mm)
Si Chip	4x4x0.33	6x6x0.33
Cu RDL	0.2x0.008	0.25x0.0065
UBM	0.19x0.0086	--
Cu Pad	0.22x0.025	0.24x0.04
SBL1	4x4x0.008	6x6x0.008
SBL2	0.0075	0.0065
PCB	8x8x0.0086	12x12x1
Low-k	4x0.005	--

Table 3 Solder ball information

Unit: mm	Ball diameter	Ball pitch	Ball counts
TV1	0.25	0.4	121
TV2	0.25	0.4	100
TV3	0.20	0.3	144
TV4	0.25	0.4	196

According to the above method, the WLP structural reliability database of different geometry combination is established for ANN analysis.

2. BOARD LEVEL RELIABILITY TEST

For the area array type WLP package, there is no underfill protection layer between the silicon wafer and the PCB, the structure is shown in Fig. 2 and the test thermal chamber is shown in Fig. 3. A mismatch in CTE (coefficient of thermal expansion) between the wafer and the PCB during thermal cycling loading may result in excessive plastic deformation of the solder balls. The strain on the solder joint caused by the thermal cycling load ultimately leads to fatigue failure. In this section, the dimensions of all four WLP test carriers are first introduced, including the size of the solder balls and the structural dimensions of each component of WLP. This study used the JEDEC thermal cycle test standard for thermal cycling testing and simulation analysis.

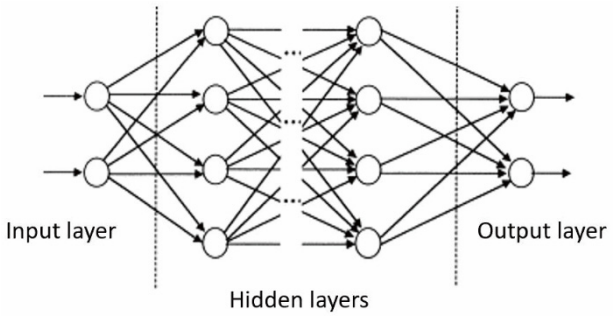
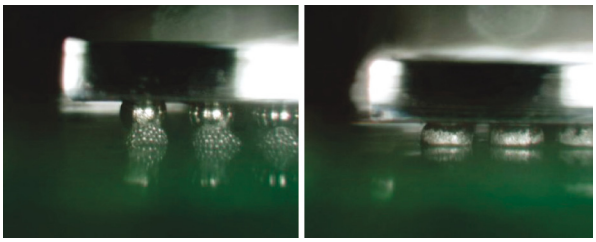


Fig. 1 Schematic of ANN.



(a) (b)

Fig. 2 WLP on PCB (a) before reflow; (b) after reflow.



Fig. 3 WLP on PCB in thermal cycling chamber.

2-1 Dimension of Test Vehicles

All four test vehicles selected were WLP. The first selected test vehicle [3], TV1, has chip size of 5.3x5.3x0.33mm with a full array layout of ball grid array, 0.4mm ball pitch and 0.25mm ball diameter, solder material is SAC. Other dimensions of the WLP are shown in Table 1. The second and third selected test vehicles [4], TV2 and TV3, have chip sizes of 4x4x0.33mm with full array layout of ball grid array. The dimensions of the two WLPs are shown in Tables 1 and 2. The last WLP test vehicle [5], TV4, has a larger chip size 6x6x0.33mm and also is a full array layout of ball grid array package. The other dimensions of the WLP are shown in Table 2. The SAC solder joint information for the four test vehicles is shown in Table 3.

2-2 JEDEC Standard for Thermal Cycling Loading

https://doi.org/10.1017/jmech.2019.20 Published online by Cambridge University Press

Table 4 Material properties of WLP

Material	Young's Modulus(GPa)	Poisson's Ratio	CTE(ppm/°C)
Solder joint	Temperature dependent	0.35	25
Silicon chip	150	0.28	2.62
Copper	68.9	0.34	16.7
Low-k	10	0.16	5
Solder mask	6.87	0.35	19
PCB	18.2	0.19	16

Table 5 Temperature dependent Young's modulus of SAC solder ball

Temperature	Young's modulus (GPa)
233K	45.74
253K	42.22
313K	31.66
353K	24.62
398K	16.70

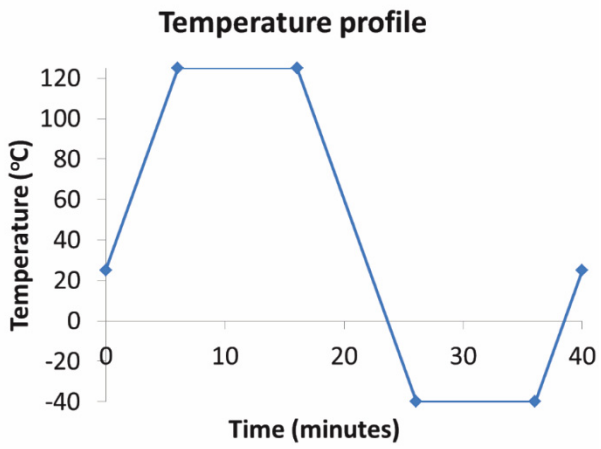


Fig. 4 Thermal cycling loading profile

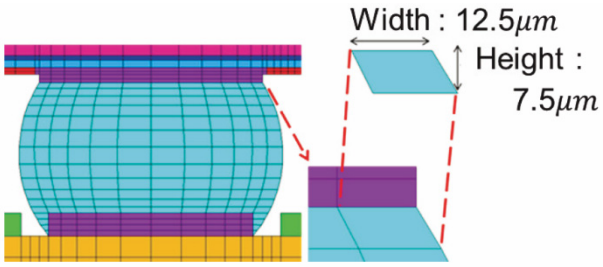


Fig. 5 The critical mesh size

The thermal cycling test conditions used in this study followed the JEDEC standard JESD22-A104D condition G [6] (temperature range: -40°C to 125°C). The rate conditions for the temperature ramping up and down both are 16.5 °C per minute. The dwell time for both high and low temperatures is fixed at 10 minutes. The thermal loading profile is shown in Fig. 4.

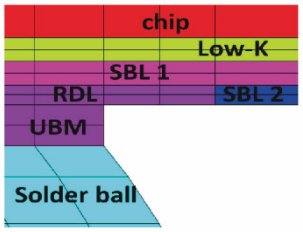


Fig.6 Schematic of FEM model of WLP structure

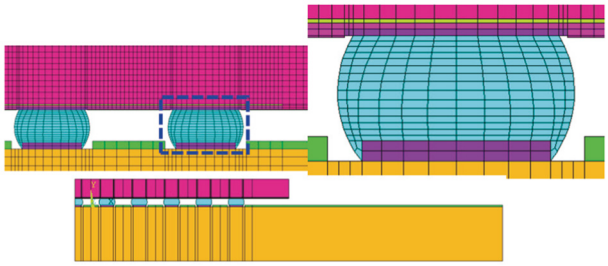


Fig.7 FEM model of TV1

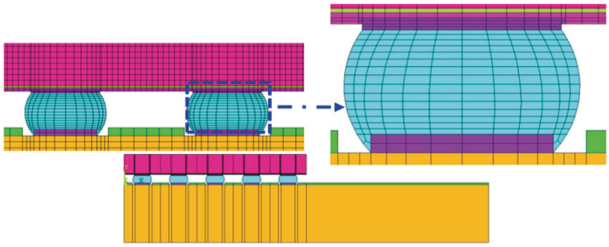


Fig.8 FEM model of TV2

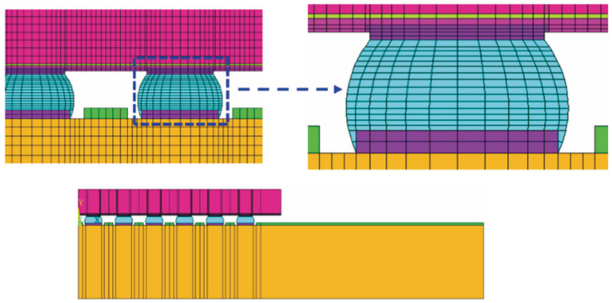


Fig.9 FEM model of TV3

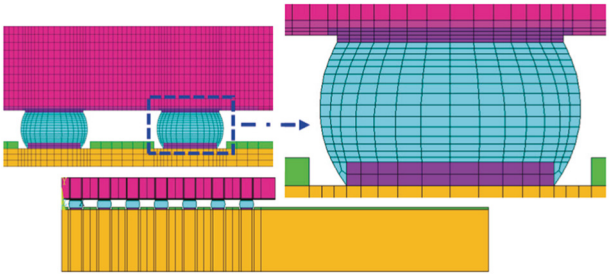


Fig.10 FEM model of TV4

https://doi.org/10.1017/jmech.2019.20 Published online by Cambridge University Press

Table 6 WLP finite element results for Coffin-Manson strain based model

Mesh size (μm) 12.5 x 7.5	Experiment data (life cycle)	FEM Coffin-Manson strain based model (life cycle)	Difference
TV1	318	295	23
TV2	1,013	970	43
TV3	876	823	53
TV4	904	876	28

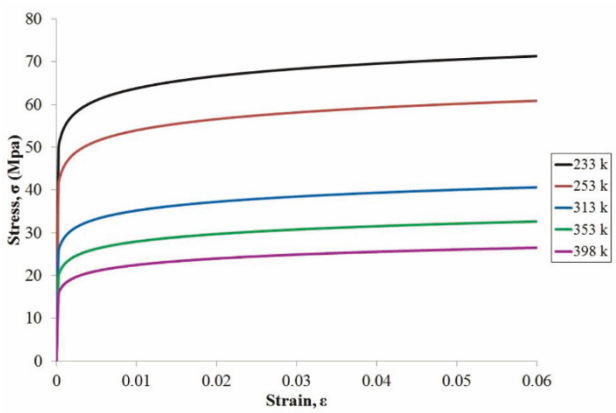


Fig. 11 Stress- strain curve for SAC solder joint [9]

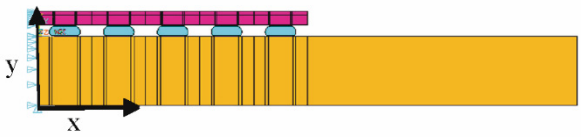


Fig.12 FEM Model Boundary Condition

3 FINITE ELEMENT SIMULATION FOR WLP

3.1 Finite Element Models

Because a large number of database to be built for machine learning, in order to perform reliability life prediction with less computation time, this study adopted a two-dimensional FEM model, this simulation methodology has a fixed mesh size at critical location, with appropriate mechanics theories and reliability life estimation empirical equation, etc. that has been validated by several thermal cycling test experiments. In order to fix the modeling pattern and analysis model of the simulation analysis, this study used the fixed mesh size at the key parts of the solder joint in Tsou [7]. However, only the solder joint size near the maximum distance from the neutral point (DNP) is fixed. As shown in Fig. 5, the height and width of the fixed mesh size are 12.5 μm and 7.5 μm, respectively. The solder joint geometry is generated by the Surface Evolver program [8], which is based on an energy algorithm. In this program, the reflow profile of the solder joint can be accurately predicted based on its surface tension, internal force, pad size and volume.

In the simulation, PLANE42 and PLANE182 were selected for the element type. Both of these are 4-node elements. In order to deal with large deformations, PLANE182 has better convergence characteristic and can be used to simulate the nonlinear plastic material properties of solder balls. Other components are all PLANE42 for linear material properties.

Figure 6 is a schematic illustration of a FEM model of WLP structure. The TV1, TV2, TV3 and TV4 FEM models are shown in Figs. 7, 8, 9, and 10. Since the structure is symmetrical, half of the structure along the diagonal is constructed.

3.2 Material Properties

The FEM model consists of a silicon chip, two stress buffer layers (SBL), a copper bump under metallurgy (UBM) layer, a low-k layer, copper redistribution line (RDL), solder joints, solder masks, and PCB structures. The individual material properties are listed in Table 4. The solder joint material curve is temperature dependent and Young's modulus under different temperature are listed in Table 5. The stress-strain curve of the SAC solder joint is shown in Fig. 11. For the curve, see Chang et al. [9], the stress-strain curve obtained by the tensile test. In ANSYS, the Chaboche kinematics hardening model is used to describe the tensile curves at different temperatures. The rest of the material properties are linear.

3.3 Boundary Conditions

Since most electronic packages are symmetrical, only half of the structure along the diagonal was modeled in this research. The x-direction displacement on each node located on the y-symmetry line is fixed to zero. In addition, all degrees of freedom of the node at the lowest point of the neutral axis of symmetry of the PCB are fixed to avoid rigid body motion. The boundary conditions of the FEM model are shown in Fig. 12.

3.4 Life Prediction Model

The life prediction model used in this study is based on the Coffin-Manson equivalent plastic strain model [10], and this model is as accurate as energy-based empirical equation [11,12]

The Coffin-Manson model is widely used in many studies since most solder joint failures are related to low cycle fatigue. The empirical Coffin-Manson equivalent plastic strain model shown in eq. (1):

$$N_f = C(\Delta\varepsilon_{eq}^{pl})^{-\eta} \tag{1}$$

Where N_f is mean cycle to failure, C and η are empirical constants, and $\Delta\varepsilon_{eq}^{pl}$ is the incremental equivalent

https://doi.org/10.1017/jmech.2019.20 Published online by Cambridge University Press

Table 7. Training data of FEM for four input parameters

Upper pad	Lower pad	Chip thickness	SBL thickness
0.18	0.18	0.20	0.0075
0.20	0.20	0.25	0.0125
0.22	0.22	0.30	0.0175
0.24	0.24	0.35	0.0225
		0.40	0.0275
(unit: mm)		0.45	0.0325

Table 8. Fifteen set of testing data

Upper Pad Diameter (mm)	Lower Pad Diameter (mm)	Chip Thickness (mm)	SBL Thickness (um)	FEM Prediction Life
0.19	0.19	0.39	10	939
0.19	0.21	0.44	9	726
0.19	0.23	0.43	8	592
0.21	0.19	0.41	27	1,265
0.21	0.21	0.36	29	1,178
0.21	0.23	0.26	19	1,008
0.23	0.19	0.23	30	1,432
0.23	0.21	0.27	21	1,319
0.23	0.23	0.42	11	866
0.20	0.22	0.37	20	945
0.22	0.24	0.42	30	993
0.24	0.20	0.43	20	1,235
0.20	0.18	.034	25	1,199
0.19	0.19	0.38	5	763
0.20	0.20	0.27	10	1,028

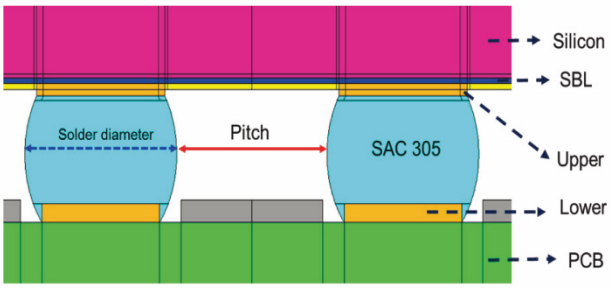


Fig.14 WLP geometry structure

plastic strain. For SAC solder joint, C and η are 0.235 and 1.75 [13].

In this research, the stabilized equivalent plastic strain after eight cycles of thermal cycling is obtained through FEM analysis by ANSYS® and this stabilized strain will be substituted into Coffin-Manson equation to predict the fatigue life of solder joint.

3.5 Life Prediction Result with Incremental Equivalent Plastic Strain

After the finite element analysis is completed, the fatigue life of WLP can be obtained by substituting the stabilized equivalent plastic strain into the Coffin-Manson equivalent plastic strain model eq. (1). The predicted fatigue life of WLP is shown in Table 6. The results show that the difference between FEM predicted life and experiment results is within a certain range. Therefore, FEM simulation technology developed in this research can be used as an alternative to experiments and can be used to build large amounts of data with much less time.

4 MACHINE LEARNING

Machine learning uses AI theory combined with big data to guide computer for training, learning and finally build a regression model. This study uses the artificial neural network algorithm implemented in Python. By training and analyzing the relationship between the input geometry parameters and the output reliability results of WLP in the database to generate the regression model, once the regression model is established, the designer only needs to input the geometry parameters of the WLP, and the predicted reliability life can be obtained immediately.

https://doi.org/10.1017/jmech.2019.20 Published online by Cambridge University Press

Table 9 Comparison of whether apply preprocessing or not

No. of Neurons	Cross validation score	
	w/o Std. preprocessing	With Std. preprocessing
5	0.8	0.95
6	0.77	0.95
7	0.81	0.97
8	0.78	0.97
9	0.81	0.97
10	0.84	0.97

Table 10 Two method of data preprocessing comparison

No. of Neurons	Cross validation score	
	Min_max	Standard Deviation (Std.)
5	0.95	0.95
6	0.96	0.96
7	0.96	0.97
8	0.97	0.97
9	0.97	0.97
10	0.97	0.97

4.1 Establishment of Dataset

WLP is composed by several components, such as solder mask, solder ball, I/O pad, buffer layer, and silicon die, etc., and the components with higher reliability effects in these structures are shown in Fig. 14. This study selected four of the most sensitive parameters to illustrate how to combine FEM, mechanics theory and AI algorithm to predict the reliability of WLP. The four design parameters used for training and learning of ANN are shown in Table 7. The total amount of data sets generated in this research for training analysis is 576. Furthermore, this study selected an additional fifteen data sets (not in the training database) to test the regression model results, as shown in Table 8.

4.2 Artificial Neural Network

Artificial neural network (ANN) method processes information by mimicking the human nervous system. As shown in Fig. 15, the data is entered at the input level, and the data in the hidden layer is calculated. After the integration is calculated, the result will be displayed in the output layer. If there are more neurons or more hidden layers in the hidden layer, the nonlinearity will be more significant. However, these adjustments also add a lot of computational complexity, overfitting, convergence problems, etc.

In the hidden layer, a_i^{ℓ} is the i_{th} activation element of the l_{th} layer. b_i^l is bias, a_i^l is equal to input value times weight w_{ji}^l and plus bias as in eq. (2):

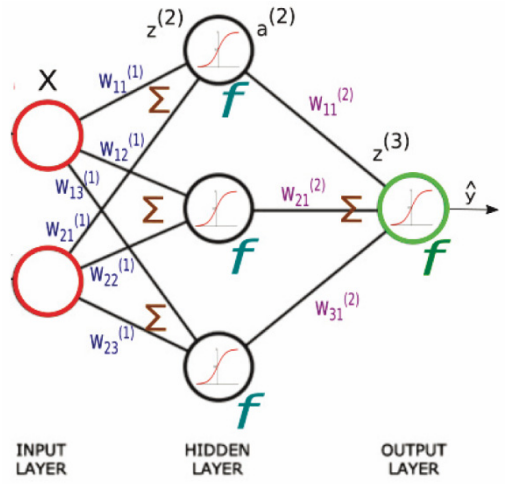


Fig. 15 Schematic of artificial neural network.

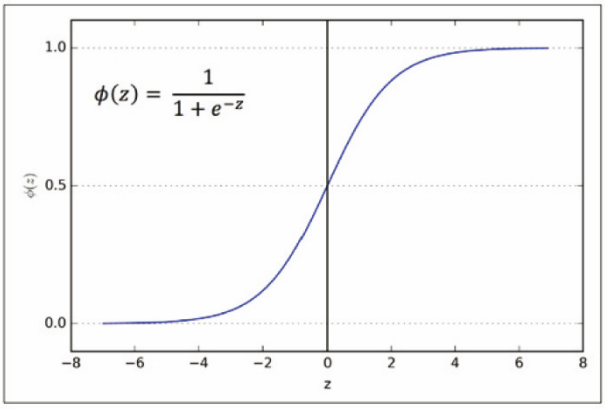


Fig. 16 Activation function-sigmoid function

$$z_i^l = \sum_{i=1}^{n} w_{ji}^l a_i^l + b_i^l \tag{2}$$

Before entering the next layer, the original value of a_i^l is substituted into sigmoid function (activation function) to be converted into a nonlinear type. As the result, we can get $a_i^{\ell+1}$ and go to the next layer.

$$a_i^{l+1} = \phi(z_i^l) \tag{3}$$

Where the activation function ϕ is shown in Fig. 16

5 RESULT AND DISCUSSION

This section will discuss how to use the artificial neural network to generate a reliable regression model of the relationship between WLP geometry and reliability life. This study will also randomly select a WLP geometry that is not in the database and input it into the regression model to estimate the reliability life of the WLP. The predicted reliability life will be compared with the FEM analysis result to demonstrate the robustness of the approach and the regression model we developed in this research.

https://doi.org/10.1017/jmech.2019.20 Published online by Cambridge University Press

Table 11 Setup of MLPregressor of scikit-learn in Python

Parameters	Attribute / Value
Function	MLPRegressor
Hidden layer	1~4 layer
Activation function	Sigmoid
Solver	LBFGS
Random state	0-300
Regularization term	10e-6
Cross validation	folds=10
Learning rate	0.001
Data preprocess	min_max_scaler
Search method	GridSearchCV

Table 12 Efficacy saturation neuron at first hidden layer

neuron in one layer	cvscore
3	96.03%
4	94.35%
5	94.51%
6	96.27%
7	96.08%
8	95.78%
9	97.19%
10	95.89%
11	96.73%
12	97.05%
13	97.71%
14	97.31%
15	97.80%
16	97.52%
17	97.32%
18	97.41%
19	97.02%
20	97.91%

5.1 Training methodology

In order to avoid data overfitting problem, this study adopted the cross-validation approach, as shown in Fig. 17. The dataset is divided into ten parts, each part could be acted as a validation or training set on different training steps, and these validation sets can also be used to predict the training results.

In order to find the best hidden layer structure, we let the input data be trained in Python, which has machine learning capabilities. Before determining the multi-layer artificial neural network function setting, it should be checked whether we should use or which kind of preprocessing method should be used. Compare the cross-validation scores without/with preprocessing methods, and the results show that data preprocessing should be used because the range of data characteristics is different. After comparing the two data preprocessing methods for min_max and standard deviation, the results showed that there was no significant difference in these pretreatment methods, but the pretreatment was significantly better than the no pretreatment. Results are shown in Tables 9 and 10.

After the data preprocessing method confirmed, the layers of the multi-layer artificial neural network are set as shown in Table 11. This study applied scikit-learn's MLPregressor in Python. The other parameters are set for the data used by the WLP database after testing. The search method, GridSearchCV, is suitable for searching for the optimal composition of random states and number of neurons. The random state is the initial weight value.

Table 13. Test set design parameters for ANN regression model

	Upper pad Dia. (μm).	Lower pad Dia.(μm)	Chip Thk. (μm)	SBL Thk. (μm)
1.	190	190	390	10
2.	190	210	440	9
3.	190	230	430	8
4.	210	190	410	27
5.	210	210	360	29
6.	210	230	260	19
7.	230	190	230	30
8.	230	210	270	21
9.	230	230	420	11
10.	200	220	370	20
11.	220	240	420	30
12.	240	200	430	20
13.	200	180	340	25
14.	190	190	380	5
15.	200	200	270	10

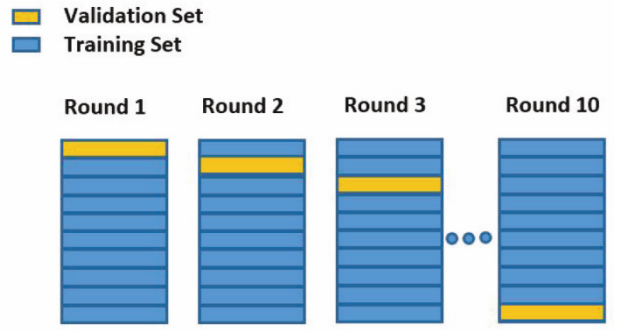


Fig. 17 Model cross validation

In order to avoid redundant neurons and save computation time, saturation test for the neuron number is performed before training. The results under 20 neuron number listed in Table 12 show that when the number of neurons reaches 13, the cross-validation score tends to gradually saturation. The amount of neurons in this study was therefore set to 20.

We selected 15 sets of design parameters not in the training database as the testing dataset to verify the robustness of ANN regression model, as shown in Table 13, and these design parameters will act as the input of each regression model, the predicted reliability life of FEA and ANN with different hidden layers and neurons are shown in Table 14. It can be seen from Table 14 that when the hidden layer increases, the difference between the ANN prediction result and the FEA prediction result can be gradually reduced, however, no matter single layer with sufficient neurons or multilayers all can predict the reliability life of WLP in an accurate range. Furthermore, although more hidden layers may have better performance,

https://doi.org/10.1017/jmech.2019.20 Published online by Cambridge University Press

Table 14 Reliability prediction results by FEM & ANN

Test No.	FEM Results	Neuron No.	Neuron No. in each layer	Neuron No. in each layer	Neuron No. in each layer
		(20)	(20,2)	(20,10,7)	(20,14,10,1)
	Reliability life prediction results by FEM & ANN				
1	939	902	917	929	951
2	726	725	722	729	725
3	592	616	616	591	589
4	1,265	1,216	1,227	1,253	1,270
5	1,178	1,183	1,171	1,179	1,178
6	1,008	1,015	1,010	1,008	1,008
7	1,432	1,431	1,448	1,431	1,434
8	1,319	1,305	1,319	1,316	1,318
9	866	886	865	862	869
10	945	937	938	944	946
11	993	1,007	989	994	993
12	1,235	1,198	1,211	1,230	1,218
13	1,199	1,197	1,206	1,197	1,197
14	763	758	762	738	772
15	1,028	1,011	1,017	1,024	1,026

the number of hidden layers increases the amount of computation for test data, reduces convergence and may cause overfitting problems.

6 CONCLUSION

This study successfully combines artificial neural network and simulation technology to create a long-term reliability database of wafer-level packages (WLPs) under various packaging sizes. ANN uses this big database for training, analysis and obtains a structure-reliability regression model for WLP. This regression model can predict the long-term reliability life of a new WLP structure immediately by simply inputting the WLP structure geometry. This methodology will greatly reduce the development time of the new WLP structure.

Multiple hidden layers of ANN can predict test data well. However, as the hidden layer increases, the computational effort will increase and might also causes overfitting problem. This study proposed a method that saves computation time and obtains the best hidden layer settings for predicting test data

ACKNOWLEDGMENT

The author is grateful for the support of the National Tsing Hua University.

REFERENCES

1. Alpaydim, E., "*Introduction to Machine Learning*", MIT Press (2014).
2. McCulloch, W. S., Pitts, W., "A logical calculus of the ideas immanent in nervous activity", *The bulletin of mathematical biophysics*, **5**, pp 115-133 (1943).
3. Hsieh, M. C. and Tzeng, S. L., "Solder joint fatigue life prediction in large size and low cost wafer-level chip scale packages," *IEEE Electronic Packaging Technology (ICEPT)*, pp. 496-501 (2015).
4. Hsieh, M. C., "Modeling correlation for solder joint fatigue life estimation in wafer-level chip scale packages", *International Microsystems, Packagings, Assembly and Circuits Technology Conference (IMPACT)*, pp. 65-68 (2015).
5. Rogers, B. and Scanlan, C, "Improving WLCSP Reliability Through Solder Joint Geometry Optimization"z *International Symposium on Microelectronics*, pp. 546-550 (2013).
6. JEDEC Standard, *JESD22-A104D*, Temperature cycling.
7. Tsou, C. Y.,Chang, T. N.,Wu, K. C., Wu, P. L. and Chiang, K. N., "Reliability Assessment using Modified energy based model for WLCSP Solder Joints", *ICEP2017*, Yamagata, Japan (2017).
8. Chiang K. N. and Yuan C. A., "An Overview of Solder Bump Shape Prediction Algorithms with Validations," *Advanced Packaging*, **24**, pp.158-162 (2001).
9. Chang, J., Wang, L., Dirk, J. and Xie, X., "Finite Element Modeling Predicts the Effects of Voids on Thermal Shock Reliability and Thermal Resistance of Power Device" , *Welding Journal*, **85**, pp. 63-70 (2006).
10. Coffin, L. F., "A study of the effects of cyclic thermal

https://doi.org/10.1017/jmech.2019.20 Published online by Cambridge University Press

stress on a ductile metal," Transactions ASME, **76**, pp. 931-950 (1954).

11. Ramachandran, V., Wu, K. C. and Chiang, K. N., "Overview Study of Solder Joint Reliability due to Creep Deformation", *Journal of Mechanics*, **34**, pp. 637-643 (2018).
12. Lee, C. H., Wu, K. C. and Chiang, K. N., "A Novel Acceleration-Factor Equation for Packaging-Solder Joint Reliability Assessment at Different Thermal Cyclic Loading Rates", *Journal of Mechanics*, **31**, Pages 35-40 (2017).
13. Xu, Y. J., Wang, L. Q., Wu, F. S., Xia, W. S. and Liu, H., "Effect of Interface Structure on Fatigue Life under Thermal Cycle with SAC305 Solder Joints," *IEEE Electronic Packaging Technology International Conference*, pp, 959-964 (2013).

(Manuscript received February 15, 2019, accepted for publication April 2, 2019.)

https://doi.org/10.1017/jmech.2019.20 Published online by Cambridge University Press